THE ASTROPHYSICAL JOURNAL, 462:1011–1019, 1996 May 10

A STUDY OF THE UNRESOLVED FINE-STRUCTURE MODEL FOR THE SOLAR TRANSITION REGION

D. SPADARO,[1] A. F. LANZA,[1] AND S. K. ANTIOCHOS[2]
Received 1995 July 10; accepted 1995 November 16

ABSTRACT

The unresolved fine-structure (UFS) model for the lower transition region was proposed by Feldman as an explanation for a number of puzzling observational results: specifically, the small filling factor of this region, the inability of the observations to resolve the temperature structure, and the observation of persistent redshifted UV emission lines even near the solar limb. It was hypothesized that opacity effects may be able to explain the redshift observations. We consider a simple model for the UFS consisting of a plasma sphere undergoing expansion and contraction due to a time-varying heating. We calculate in detail the line profile of the well-observed C IV 1548 Å line. Our calculations include the effects of both nonequilibrium ionization and radiative transfer. We find that although the model can reproduce some of the features of the observations, such as the line widths, the effect of finite optical depth is to produce a blueshifted peak for the emission line, contrary to observations. The physical origins of this blueshift are discussed. We conclude that unless the pressures of the UFS are significantly higher than the typical pressures assumed for the lower transition region, opacity effects are unlikely to explain the observations.

Subject headings: Sun: transition region — Sun: UV radiation

1. INTRODUCTION

Ultraviolet (UV) and extreme ultraviolet (EUV) observations of the Sun and of late-type stars have shown that the emission lines originating in the transition region, at $T \sim 10^5$ K, exhibit persistent redshifts (Doschek, Feldman, & Bohlin 1976; Lites et al. 1976; Gebbie et al. 1981; Ayres et al. 1983; Dere, Bartoe, & Brueckner 1984; Ayres, Jensen, & Engvold 1988; Athay & Dere 1989). In addition, the lines have almost Gaussian profiles that are broadened in excess of the thermal widths corresponding to the line formation temperature in ionization equilibrium (Brueckner & Moe 1972; Boland et al. 1975; Doschek et al. 1976). For the Sun, the emission pattern appears to be steady for days and occurs in all regions: coronal holes and quiet and active regions.

Interpreting the line redshifts as due to a downflowing plasma, the velocities required to produce the shifts are of the order of 10 km s^{-1} at 10^5 K. They decrease both at lower and higher temperatures (Dere 1982). A controversial question concerns the center-to-limb variations of the redshifts. If the lines are due to optically thin emission, then from simple geometric arguments one would expect the redshifts to vary on average as the cosine of the solar longitude, so that the shifts should vanish at the limb. A study of active regions by Feldman, Cohen, & Doschek (1982), however, suggests that, although they may decrease by a factor of about 2 near the limb, the redshifts do not vanish there. On the other hand, the analyses by Athay & Dere (1989) and Henze & Engvold (1992) are in favor of a vanishing of the redshifts toward the limb. Klimchuk's (1987) analysis of *Solar Maximum Mission* (*SMM*) data may provide the resolution to this discrepancy. He concludes that in active regions the line shifts persist out to the limb, but that in quiet regions the line shifts do vanish at the limb.

The broadening of the emission lines above their thermal widths is commonly interpreted as due to a distribution of randomly oriented velocities. Lines formed at increasingly higher temperatures exhibit higher nonthermal mass motions: at 10^5 K, the nonthermal mass motions reach a value of about 20 km s^{-1} (e.g., Doschek et al. 1976; Feldman, Doschek, & Patterson 1976). Data at coronal temperatures are very limited, but it appears that at some temperature in the upper transition region the nonthermal velocity must peak and then either remains roughly constant (Hassler et al. 1990) or begins to decline (Cheng, Doschek, & Feldman 1979). A basic property of this broadening is that its magnitude appears to be largely independent of the spatial resolution of the observations; hence, it must be due to motions on a length scale smaller than 2000 km (Dere 1989).

Several models have been proposed to describe the dynamics of the transition region plasma. An important constraint on the models is that the mass flux estimated from the redshift observations is sufficient to empty the corona in a few days; therefore, it seems highly unlikely that a net downward mass flux is the only motion involved. There must be an upflow that balances most of the observed downward flow. The apparent downflow must result from a spatial and/or temporal averaging of the motion of material which is more visible at UV wavelengths when descending than when ascending.

Models assuming a steady global circulation of material between the chromosphere and the corona and a steady state plasma heating, either spatially uniform or strongly localized, do not appear to be compatible with the observed line shifts. Specifically, investigations based on steady siphon-flow loop models with uniform energy input cannot account for the observed line shifts in the transition region, because the blueshifted emission coming from the upflowing leg of the loop dominates over the redshifted emission from the downflowing leg (Antiochos 1984; Spadaro et al. 1990). Other authors have argued that the redshifts can be produced by steady state loop models in which a strong spatial dependence of the energy input is

[1] Osservatorio Astrofisico di Catania, Città Universitaria, Catania, Italy.
[2] E. O. Hulburt Center for Space Research, Naval Research Laboratory, Washington, DC.

introduced, but very extreme assumptions are required to reproduce the observed velocities and line intensities (McClymont & Craig 1987; Mariska 1988; McClymont 1989). In particular, the location of the dissipation region must be very close to the base of the loop and its spatial extent must be much smaller than the loop's length scale. Also, the magnitude of the heating and the size of the loops are highly constrained (McClymont & Craig 1987; Mariska 1988).

In the light of such difficulties with steady heating models, it is worthwhile to consider the hypothesis that the solar transition region and corona are heated by an episodic rather than a steady process. In fact, a small-scale stochastic heating is suggested by the accumulating observational evidence for ubiquitous small-scale transient activity in the ultraviolet and X-ray emission (Brueckner et al. 1986; Habbal & Withbroe 1981; Porter, Toomre, & Gebbie 1984). According to this picture, Parker (1988, 1989) has proposed that the global heating of the solar corona is provided by a more or less unresolved population of "nanoflares." Also, Sturrock et al. (1990) assumed that "microflares" instantaneously deposit enough energy to heat a small element of gas to some temperature, and that all the observed coronal and transition region emission arises in the subsequent cooling (with no thermal conduction or continued heating) of such impulsively heated gas.

Other authors (Athay 1984; Athay & Holzer 1982; Blake & Sturrock 1985; Cheng 1992a, b, c), have considered the possibility that the coronal heating may be due to spicule activity. The flow signatures detected in the transition region emission lines are interpreted as a consequence of the dynamic processes associated with the transient acceleration and heating of chromospheric plasma. The line redshifts, in particular, would be produced by plasma structures undergoing cooling and condensing back onto the chromosphere.

The extensive observational and theoretical work cited above leads us to reconsider the proposal by Feldman (1983, 1987) that most of the solar radiation detected in emission lines formed in the (3–50) $\times$ 10^4 K temperature range is produced in plasma structures magnetically isolated from the chromosphere and corona. These structures are characterized by a gas pressure about an order of magnitude higher than the surrounding atmosphere. The size of such structures should be extremely small and, as yet, unresolved by current space instrumentation. Feldman called these entities "unresolved fine structures" (UFSs).

In this work we formulate quantitative models for the UFSs proposed by Feldman and calculate the characteristics of the predicted line emission. Our goal is to determine whether these models are able to reproduce the observed properties of the solar transition region emission lines, particularly the flow signatures (line shifts, broadening, asymmetries), when the nonthermal energy supply to the plasma confined in these structures occurs impulsively.

2. A MODEL FOR UNRESOLVED FINE STRUCTURE

In a previous paper (Antiochos 1990), we have argued that since the magnetic field in the network is observed to have a highly mixed polarity, the field in this region must consist of a complex system of separatrix surfaces and magnetic null points. One attractive possibility for the nature of the UFS is that it is high-beta plasma that collects at the nulls, and is heated by bursty reconnection there (e.g., Priest 1986). Some support for this picture can be found in the recent *Yohkoh* observations, which indicate that much of the flare X-ray emission originates in bright knots near the tops of flare loops (e.g., Doschek, Strong, & Tsuneta 1995). In the usual model for two-ribbon flares, (e.g., Sturrock 1966), this is also the location of a Y-type null point. We propose that the heating of the lower transition region may be due to many small flarelike events, which also involve reconnection at null points.

The geometry of the null-point plasma is likely to be complicated, but the essential physics can be captured by assuming that a UFS consists of a sphere of field-free plasma of radius R, electron density n_e (equal to the proton density n_p), and temperature T, surrounded by a magnetically dominated external region. Note that the magnetic field prevents the effective interchange of both mass and heat between the UFS and its surroundings, even parallel to the field, because of the rapid increase of field strength with increasing distance from the null. The density and temperature are taken to be uniform inside the UFS and depend only on time t.

The evolution of the UFS radius R is determined by the balance between the gas pressure p inside the sphere and the pressure of the external magnetic field. In order to calculate the evolution of this field, a full MHD simulation is required; hence, we simply parameterize the external magnetic pressure according to $B^2/(8\pi) = p_0(R/R_0)^\alpha$, where B is the external confining field, p_0 is the pressure corresponding to the initial radius R_0, R is the radius at time t, and α is a free parameter depending on the specific geometry of the field. For example, near an X-type neutral point of a current-free field, we would expect that $\alpha = 2$, since B will in general vary linearly with radius near the null (e.g., Fukao, Masayuki, & Takao 1975).

The evolution of the UFS density n_e is determined from mass conservation, and the temperature T is determined by the energy equation. The energy loss terms are the work done in expanding against the external field, and radiation cooling, which is treated by using the optically thin loss function (e.g., Gaetz & Salpeter 1983).

Under these assumptions, the mass, momentum, and energy conservation equations for our model reduce to:

$$\frac{4\pi}{3} n_e R^3 = \text{constant} , \tag{1}$$

$$2kn_e T = \frac{B^2}{8\pi} = p_0\left(\frac{R}{R_0}\right)^\alpha , \tag{2}$$

$$\frac{3}{2}\frac{dp}{dt} + \frac{5p}{2r^2}\frac{\partial(r^2 v)}{\partial r} = \epsilon_h - L_r , \tag{3}$$

where k is Boltzmann's constant, r is the radial coordinate measured outward from the center of the sphere, ϵ_h is the heating rate per unit volume, L_r is the radiative cooling rate per unit volume, and v is the velocity of the plasma. Note that since we expect the velocity to be well below the sound speed c_s, we have dropped the kinetic energy term in equation (3) and neglected all spatial gradients in the pressure. We assume a form for the heating

$$\epsilon_h = \epsilon_0\left(\frac{n_e}{n_{e0}}\right) g(t) , \tag{4}$$

where ϵ_0 is the initial heating rate at the starting density n_{e0} and $g(t)$ describes the temporal evolution of the heating

[$g(0) = 1$]. The radiative losses are given by

$$L_r = n_{e0}^2 \left(\frac{n_e}{n_{e0}}\right)^2 \Lambda_0 f(T) , \quad (5)$$

where $\Lambda_0 f(T)$ is the radiative cooling function (e.g., Gaetz & Salpeter 1983), with $\Lambda_0 = 10^{-21}$ ergs cm^3 s^{-1}.

Equation (3) can be integrated over the sphere, giving

$$3kn_e \frac{dT}{dt} + 15kn_e T \frac{1}{R}\frac{dR}{dt} = \epsilon_h - L_r . \quad (6)$$

Then equations (1), (2), and (6) can be combined to give an ordinary differential equation for the relative radius of the sphere $\varrho \equiv R/R_0$:

$$\frac{d\varrho}{dt} = \frac{1}{t_h} g(t) \varrho^{-(\alpha+2)} - \frac{1}{t_c} \varrho^{-(\alpha+5)} f(T) , \quad \text{with } \varrho(0) = 1 , \quad (7)$$

where

$$t_h = \frac{(24 + 3\alpha)p_0}{2\epsilon_0} , \quad (8)$$

and

$$t_c = \frac{(24 + 3\alpha)p_0}{2\Lambda_0 n_{e0}^2} , \quad (9)$$

are the heating and the cooling timescales, respectively. These are determined by the initial conditions and the parameter α. Solving equation (7) for ϱ, the evolution of the density and temperature follows from $n_e = n_{e0}\varrho^{-3}$ and $T = T_0 \varrho^{(\alpha+3)}$, respectively. In addition, the plasma velocity v can be deduced from the continuity equation, $dn_e/dt + n_e \nabla \cdot \boldsymbol{v} = 0$:

$$v(r) = r \frac{1}{\varrho}\frac{d\varrho}{dt} . \quad (10)$$

An example of the evolution of temperature, density, radius, and surface velocity of our UFS model for a particular set of parameters is shown in Figure 1. The assumed parameters are $\alpha = 2$, $\epsilon_0 = 10$ ergs cm^{-3} s^{-1}, and the initial values $T(0) = 3 \times 10^4$ K, $n_{e0} = 8 \times 10^{10}$ cm^{-3}, and $R_0 = 1.8 \times 10^7$ cm. These parameters imply that $t_h = 1.0$ s and $t_c = 3.0$ s. The function $g(t)$, appearing in the expression of the heating rate per unit volume, is assumed to have the form $g(t) = 1$ for $0 \le t \le 0.7$ s, $g(t) = 0$ for $t > 0.7$ s.

Note that the form for the heating, equation (4), implies that for constant $g(t)$ the rate of total energy input to the UFS is constant. Hence the total energy release is given by $(4\pi/3)R_0^3 \epsilon_0 \Delta t$, where Δt is the duration of the heating. For the parameters above, this energy is only 1.7×10^{23} ergs, which can be easily be supplied by a small volume of network magnetic field ~ 30 G. It is also of the order of the "nanoflare" energy postulated by Parker (1988, 1989).

In Figure 1 the expansion velocity at $t = 0$ jumps to a high value because we have neglected the inertial terms in the momentum equation; consequently, the UFS plasma reacts immediately to the instantaneous "switching on" of the heating. During the energy input phase (0 s $\le t \le$ 0.7 s), the model is only approximately valid, since the velocity of expansion is comparable to the sound speed. For $t > 0.7$ s, there is no further energy input, and the plasma enters a cooling phase dominated by the radiative losses. As a result of the decrease of gas pressure, the sphere begins to contract. This contraction phase is well described by our model, since $v \ll c_s$. Note that the highest contraction velocities occur at around $T = 10^5$ K, where the radiative losses are also maximum (e.g., Gaetz & Salpeter 1983).

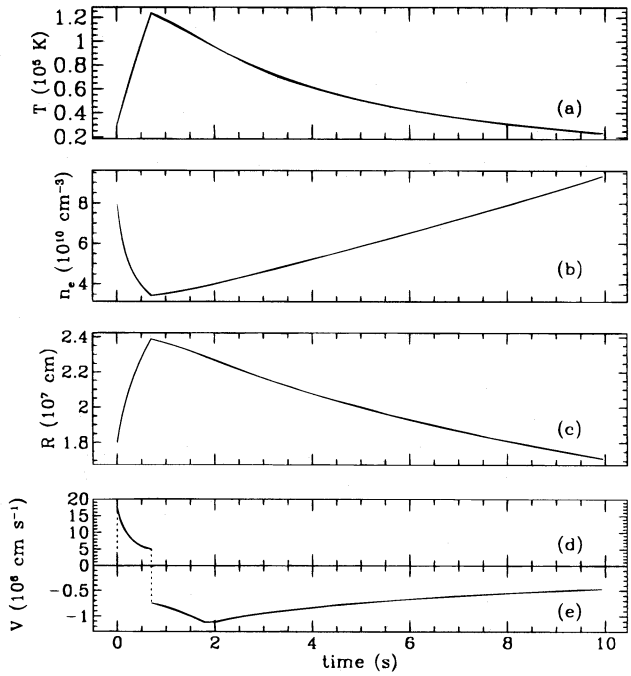

FIG. 1.—(*a*) Temperature T, (*b*) electron density n_e, (*c*) radius, and (*d*, *e*) surface radial velocity v vs. time t for the UFS model. Note that two different scales have been adopted to plot expansion velocities ($V > 0$) and contraction velocities ($V > 0$) in panels *d* and *e*, respectively.

An important issue is the sensitivity of the UFS evolution to the magnitude of the parameters, ϵ_0 and Δt, assumed for the heating. As a first approximation, we neglect the radiative losses during the heating phase and integrate equation (7) over the duration of the heating to find that at the end of the heating phase, $R \propto (\epsilon_0 \Delta t)^{1/(\alpha+3)}$, $n \propto (\epsilon_0 \Delta t)^{-3/(\alpha+3)}$, and $T \propto \epsilon_0 \Delta t$. We conclude that if $\alpha = 2$, the UFS radius is highly insensitive to the magnitude of the heating, which would imply that the structures are unlikely to be resolved even for large heating. The density is only weakly dependent on heating, but the maximum temperature scales vary approximately linearly with the total energy released. Consequently, the magnitude of the energy release must fall within a somewhat narrow range $\sim 10^{23}$ ergs in order for the model to be applicable to the transition region.

3. LINE PROFILES

We have calculated the line profiles expected from the UFS model of Figure 1 for ultraviolet emission lines collisionally excited from the ground level. We have not used the usual approximation of optical thinness, but have taken into account opacity effects in the line formation process, because the plasma density inside the examined structure is about an order of magnitude higher than the value often considered for the standard solar transition region (Feldman 1983, 1987). Moreover, we wish to test the hypothesis that the observed line shifts might be explained

as a consequence of line opacity in pulsating spherical structures, in which the emitting plasma is brighter during contraction than during expansion (Feldman 1983).

The geometry of the simulated observations is shown in Figure 2, where the x-axis is parallel to the observer's line of sight. For a given line of sight, expressing the line specific intensity I as a function of the difference $\Delta\lambda = \lambda - \lambda_0$ with respect to the line rest wavelength λ_0 (measured in angstroms), we have

$$I(\Delta\lambda) = \int_{-x_0}^{x_0} F_0(x)\varphi_e(\Delta\lambda, x) \exp\left[-\tau(\Delta\lambda, x)\right]dx , \quad (11)$$

where the limits of the integral correspond to the intersections of the selected line of sight with the surface of the sphere. $F_0(x)$ is the contribution function, $\varphi_e(\Delta\lambda, x)$ is the emission profile, and $\tau(\Delta\lambda, x)$ is the optical depth at wavelength λ. We evaluate the function $F_0(x)$ by adopting the escape probability method, in order to take into account the contribution of the scattered photons to the line emissivity (Hummer & Rybicki 1982; Rybicki 1984; Meier 1991). Hence we assume that

$$F_0(x) = \frac{j_0}{E(r)} , \quad (12)$$

where j_0 is the total emissivity for a collisionally excited resonance line and $E(r)$ is the escape probability for line photons at radius r, i.e., the probability averaged over wavelengths and directions that a photon will escape the sphere from a point at radius r without being scattered (or absorbed). In fact, the approximation adopted in equation (12) is better the more uniform $E(r)$ is over the sphere (see Meier 1991; Rybicki 1984). [We refer the reader to Rybicki 1984 for details on the determination of $E(r)$]. The emissivity is given by, e.g., Landini & Monsignori-Fossi (1990) and references therein:

$$j_0 = 2.17 \times 10^{-16} f n_i n_e T^{-1/2} g(T) 10^{-5040W/T} \times \text{ergs cm}^{-3}\ \text{s}^{-1}\ \text{sr}^{-1} , \quad (13)$$

where f is the oscillator strength of the transition, n_i the number density of the emitting ions, $g(T)$ the effective Gaunt factor, and W the excitation energy of the transition (in eV). We assume excitation from the ground level and that all the ions are in that level.

The emission profile in equation (11) is assumed to be Gaussian:

$$\varphi_e(\Delta\lambda, x) = \frac{1}{\sqrt{\pi}\,\Delta\lambda_D} \exp\left[-\left(\frac{\Delta\lambda - \lambda_x}{\Delta\lambda_D}\right)^2\right] , \quad (14)$$

where $\Delta\lambda_D$ is the Doppler half-width of the line:

$$\Delta\lambda_D = \frac{\lambda_0}{c}\left(\frac{2kT}{m_i}\right)^{1/2} , \quad (15)$$

where k is Boltzmann's constant, c the velocity of light, and m_i the mass of the ion producing the spectral line. The quantity $\lambda_x = \lambda_0 v_{ls}/c$ is the Doppler shift introduced by the component of the flow velocity along the observer's direction, v_{ls}, in each point along the line of sight.

The line optical depth $\tau(\Delta\lambda, x)$ is given by

$$\tau(\Delta\lambda, x) = \int_x^{x_0} \chi_0\, \varphi_a(\Delta\lambda, s) ds , \quad (16)$$

where $\varphi_a(\Delta\lambda, s)$ is the absorption profile, assumed equal to the emission profile, and the absorption coefficient χ_0 is given by (e.g., Gray 1992; Mariska 1992),

$$\chi_0 = n_i \frac{\pi e^2}{m_e c^2} \lambda_0^2 f , \quad (17)$$

where e and m_e are the electron charge and mass, respectively.

For the number density of the ionic species involved in the radiative transitions, n_i, we do not use the values calculated under the usual approximation of ionization equilibrium, because the temperature and electron density vary in our model on timescales of the order of a second or less. This time is shorter than the characteristic ionization and recombination timescales of most of the relevant ions; therefore, we determine the densities of the emitting ions by solving the time-dependent ionization balance equations (e.g., Raymond 1979, 1990; Doyle et al. 1985). We adopt the collisional ionization coefficients and the radiative and dielectronic recombination coefficients given by Arnaud & Rothenflug (1985). The balance equations are solved by assuming ionization equilibrium at $t = 0$ and then using the temperature and electron density evolution given by the hydrodynamic model of § 2. Finally, the line intensities evaluated from equation (11) for each line of sight are averaged over the apparent disk of the UFS. This yields an intensity value that can be compared directly to the available observations, which are characterized by a spatial resolution about an order of magnitude larger than the assumed UFS radius.

As a specific application of the described model, we present a series of computations of the profile of the C IV

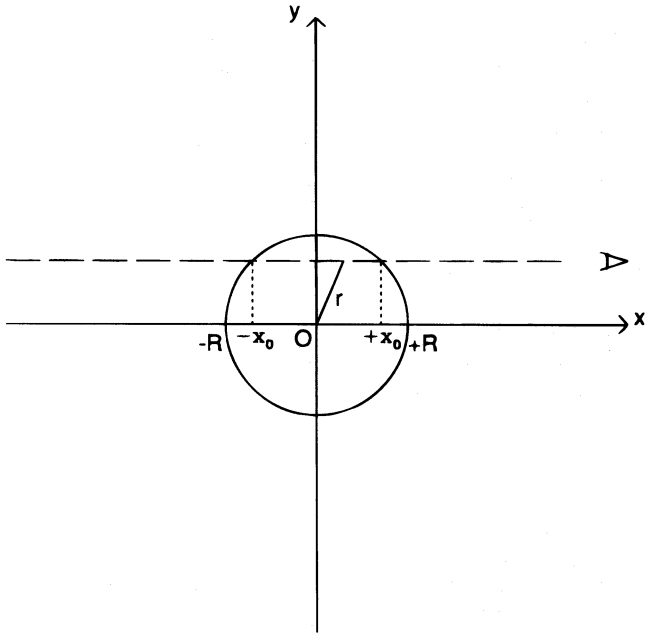

FIG. 2.—Sketch of the UFS geometry adopted in modeling line profiles. The UFS center is at O, its surface radius is R, while r is the radial distance of a plasma element from the center O. For a given line of sight (*dashed*) the abscissae of the intersections with the surface are labeled $-x_0$ and $+x_0$, respectively.

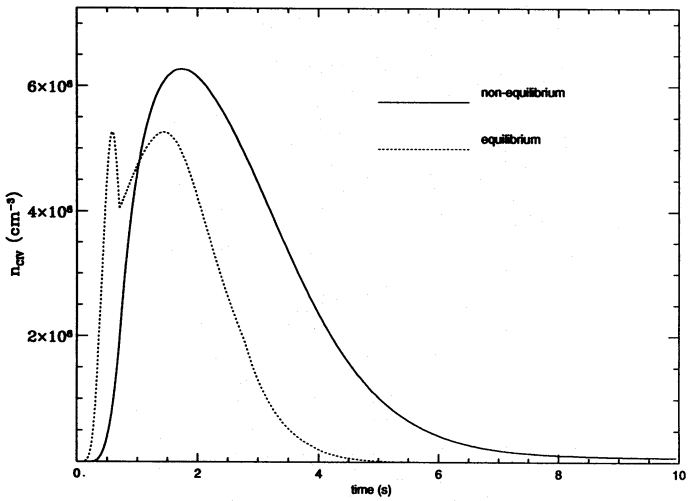

FIG. 3.—Number density of the C IV ion vs. time t. The continuous line indicates the actual ion density computed from the time-dependent ionization balance equations for the UFS model in Fig. 1, while the dotted line indicates the ion density computed for the same model assuming ionization equilibrium.

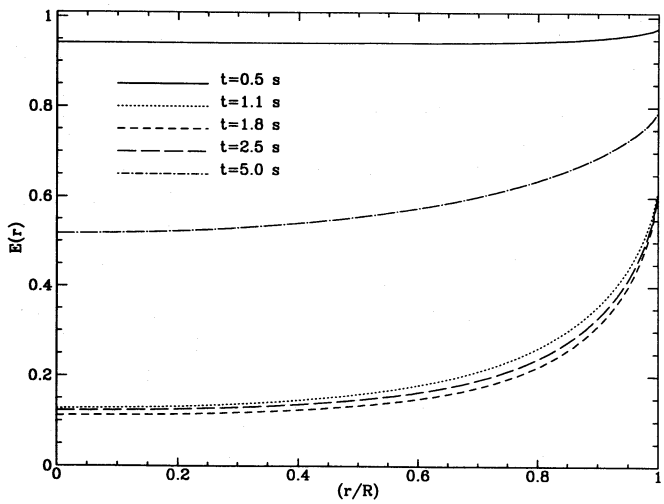

FIG. 4.—Escape probability $E(r)$ vs. the relative radial coordinate r/R at various times t for the considered UFS model. The different line types indicate the times as labeled.

λ1548.2 line, using the temporal variations of temperature, density, and velocity previously calculated in § 2 (see Fig. 1). First, we show in Figure 3 the number density of C IV versus time; the same ion density calculated under the assumption of ionization equilibrium is shown for comparison. The equilibrium density is essentially a function of temperature only and follows its variation, peaking at $\sim 10^5$ K (Arnaud & Rothenflug 1985). The actual ion density departs considerably from the equilibrium value. C IV is up to 2 orders of magnitude underabundant during the impulsive heating phase, owing to the inertia of the ionization processes from the lower ionization stages. Conversely, it is considerably overabundant during the cooling phase, because of the inertia of recombination to the lower stages.

We have computed the instantaneous escape probability and the corresponding line profiles and total intensities at five times, adopting the atomic parameters reported by Landini & Monsignori-Fossi (1990) and references therein. The escape probability is plotted versus UFS radius and time in Figure 4. Its behavior can be understood from the fact that it depends not only on position but also on the velocity field inside the sphere, because the emission and absorption profiles of the plasma elements are shifted with respect to each other according to their relative velocities. We note that during the rapid expansion phase, at $t = 0.5$ s, the Sobolev limit is approached and $E(r)$ is nearly constant and almost unity (Rybicki 1984). Also, in the other cases $E(r)$ is almost constant over most of the sphere radius, justifying the approximation adopted in equation (12). Only in the outermost shell of the sphere does $E(r)$ vary significantly and the approximation become less valid.

The C IV λ1548.2 total intensities and profiles at five times are reported in Table 1 and Figure 5. At $t = 0.5$ s, during the heating phase, the total intensity is $\sim 2.7 \times 10^4$ ergs cm^{-2} s^{-1} sr^{-1}. The profile is very nearly symmetric with a line half-width of ~ 0.2 Å. During the cooling phase, the line intensity is about an order of magnitude higher. The line profile is asymmetric with a blueshifted peak and an extended tail on the red wing. The line half-width is between ~ 0.1 and ~ 0.15 Å, and is maximum around $T = 10^5$ K ($t = 1.8$ s). At $t = 5.0$ s, the profile is again symmetric, with a negligible line shift and a line half-width of ~ 0.05 Å, about 2 times narrower than earlier in the cooling phase.

4. DISCUSSION

When comparing the results of the above model to the C IV line observations, it should be emphasized that the observed properties of the solar transition region are due to a summation over a distribution of UFSs, with different density, radius, and maximum temperature at the end of the impulsive heating phase. Any model for the UFS distribution, however, requires knowledge of the coronal heating mechanism, which is poorly understood at present. As a first step, we consider in this paper only the time-averaged properties of the representative model calculated above, and compare these results with the data.

The total intensities reported in Table 1 show that most of the C IV line emission from the model occurs during the cooling phase, which tends to have the longest duration. For any particular value of temperature and density, the C IV intensity during the cooling (contraction) phase is considerably higher than that calculated for the heating (expansion) phase. This result is due to the nonequilibrium ionization effects that occur in UFS plasma undergoing fast temperature variations: the underabundance of C IV during the impulsive heating phase (see Fig. 3) significantly depletes the relevant line emission, while the ion over-

TABLE 1

C IV λ158.2 TOTAL INTENSITIES AND PROFILES

Time (s)	Temperature (10^4 K)	Total Specific Intensity (10^4 ergs cm^{-2} s^{-1} sr^{-1})
0.5.....	9.80	2.67
1.1.....	11.56	37.47
1.8.....	9.97	46.06
2.5.....	8.44	39.08
5.0.....	5.06	5.11

abundance characterizing the radiative cooling phase enhances the emission. Therefore, nonequilibrium effects appear to be the crucial factor determining the difference in total line emission between the expansion and the contraction of the sphere. This result is general and should apply to any ion whose equilibrium temperature of maximum fractional population is not much lower than the maximum temperature reached by the UFS plasma before beginning radiative cooling.

In addition to producing a higher emission during the cooling phase, the contraction of the UFS can explain the observed magnitude of the nonthermal line broadening. Dere et al. (1987) obtained an average line width of 0.195 Å from a set of measured C IV line profiles. This value is comparable to that shown in Figures 5*b*–5*c*. Our model produces a broadening which is maximum around 10^5 K, because the radiative losses are maximum at that temperature, yielding the highest contraction velocity [cf. eq. (7) with $g(t) = 0$].

The main difficulty with our model is that it is not able to reproduce the observed line shifts, since the profile peak is blueshifted during the cooling phase. This result can be understood from the fact that the emission comes predominantly from the inner region of the sphere where $E(r)$ is lower, whereas the absorption is dominated by the external shell. Since the external shell is contracting, the maximum of the absorption in the observer's reference frame occurs at a wavelength longer than the rest wavelength λ_0, thereby producing a depression of the red wing of the profile and a relative enhancement of the blue wing. The tail on the red wing of the line is due to emission from the front side of the external shell, i.e., nearest to the observer.

We can quantify these ideas by deriving an expression for the difference of the intensities at two wavelengths that are symmetrically located with respect to the rest wavelength, $\Delta I(\Delta\lambda) = I(\Delta\lambda) - I(-\Delta\lambda)$ (see the Appendix):

$$\Delta I(\Delta\lambda) = 2\,\frac{\exp(-\tau_m/2)}{\chi_0}\int_0^{\tau_m} F_0(\tau)\sinh(\tau_m/2 - \tau)d\tau\,, \quad (18)$$

where the contribution function F_0 has been expressed in terms of the optical depth τ at $\Delta\lambda$, and $\tau_m(\Delta\lambda) = \int_{-x_0}^{x_0} \chi_0\,\varphi_a(\Delta\lambda, s)ds$ is the total optical depth along the given line of sight.

When $\Delta I(\Delta\lambda) > 0$ for each $\Delta\lambda$, the red portion of the profile dominates; when $\Delta I = 0$; we have an unshifted, sym-

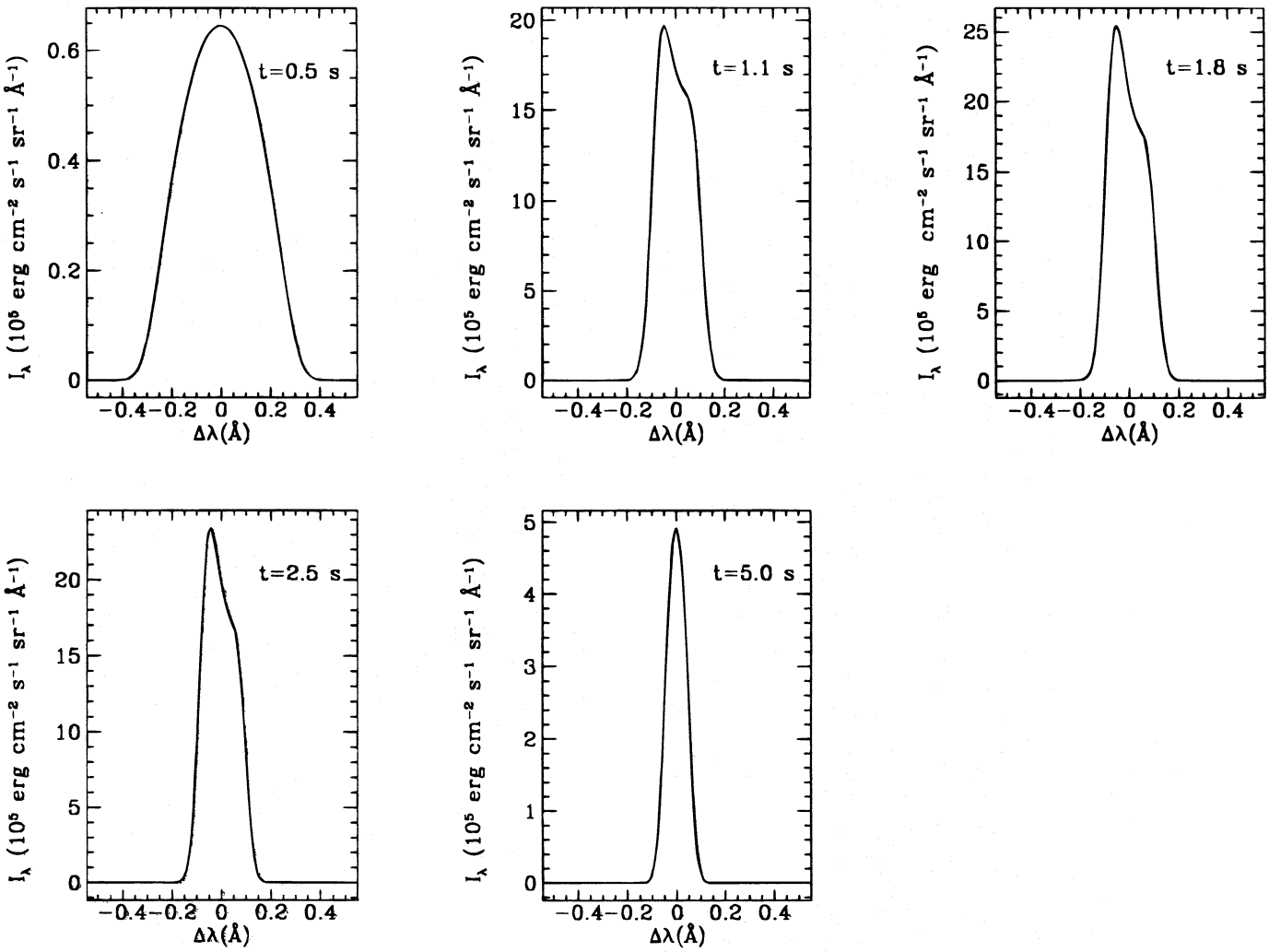

FIG. 5.—Line profiles computed for the considered UFS model at the times t indicated inside each panel, respectively. The intensity I_λ is the average of the specific intensity over the UFS disk (see the text) and is reported as a function of the relative wavelength $\Delta\lambda = \lambda - \lambda_0$, where $\lambda_0 = 1548.2$ Å is the rest wavelength of the line.

metric line profile; and when $\Delta I < 0$, the blue portion dominates. For a uniform contribution function [i.e., $F_0(\tau) =$ constant] the line profile is symmetric for all lines of sight, because the integral over τ in equation (18) vanishes; hence, averaging over the lines of sight yields a symmetric profile. This is the case for the profile computed at $t = 0.5$ s, since the escape probability is almost constant and nearly unity throughout the sphere. On the other hand, during the cooling phase, $F_0(\tau)$ is not uniform because the escape probability is expected to be lower at the center of the sphere. In Figure 6*a* a typical plot of the function $F_0(\tau)$ is given for a contracting sphere, together with that of the factor $\sinh(\tau_m/2 - \tau)$ and the product $F_0 \sinh(\tau_m/2 - \tau)$. In this case the center of the sphere (i.e., the point at which F_0 reaches its maximum) has $\tau = \tau_c > \tau_m/2$, as is illustrated in Figure 6*b*. Therefore, the integral in equation (18) is negative for all $\Delta\lambda$'s and all the lines of sight (see Fig. 6*a*), so that the resulting line profile is blueshifted.

When the temperature gets below $T = 10^5$ K, the blueshift begins to decrease, until around $t = 5.0$ s, near the end of the cooling phase, the profile is again symmetric. This can be interpreted as the combined effect of a reduced opacity, due and the much lower C IV density, and a slower contraction.

It is interesting to determine what kind of modifications are needed in the present model in order to reproduce the observed line redshifts, while still maintaining the attractive feature of explaining nonthermal line broadening. The qualitative behavior of line profiles can be studied using equation (18), which holds whenever the velocity field is radial and spherically symmetric around the center of the sphere (not necessarily with $dv/dr =$ constant as in our model) and F_0 depends only on r. In order to have a redshift during contraction, as suggested by Feldman (1983), the line emissivity at the center of the UFS sphere must have a value at least 3–5 times lower than that in the external shell, so as to compensate for the effect of the decreasing escape probability. This implies, however, a nonuniform UFS model in which density and/or temperature are significantly higher in the external shell of the sphere. We would have to abandon the hypothesis of spatial uniformity with a drastic modification of the model and a significant increase in the difficulty of the calculation. Given the character of the present approach, we defer such an analysis to subsequent work.

Another possibility is to include continuum absorption, which can occur if we assume the presence of cooler plasma, with a temperature ~ 5000 K, inside the sphere. Continuum absorption due to cool matter would reduce the line radiation received from the far side of the contracting sphere, which mainly contributes to the blue portion of the profile, so that the redshifted emission from the side of the shell in front of the observer would dominate. However, adopting the continuum absorption coefficient at $\lambda = 1548.2$ Å given by Vernazza, Avrett, & Loeser (1976) for the temperature minimum region of the solar atmosphere, and even taking into account the absorption by some molecular bands of CO (Dragon & Mutschlecner 1980), a column density of order 10^{20}–10^{21} cm^{-2} is required to provide an optical

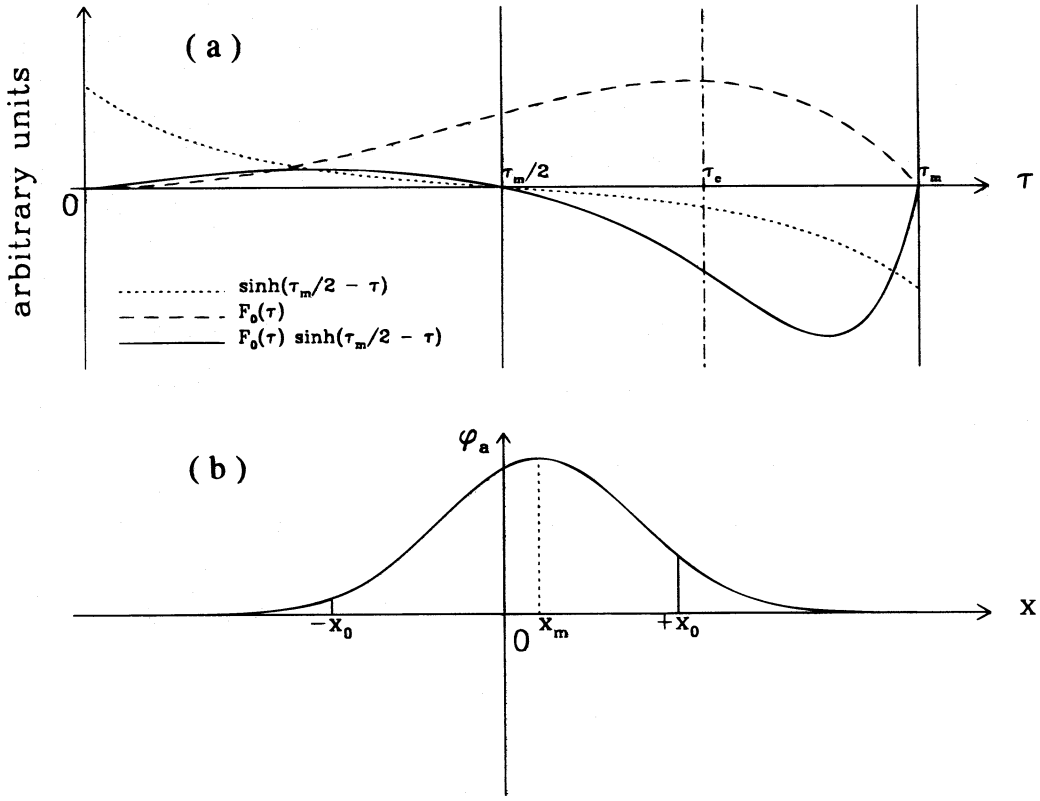

FIG. 6.—(*a*) Qualitative plots of the integrand $F_0(\tau)\sinh(\tau_m/2 - \tau)$ in eq. (18) and of the two factors F_0 and $\sinh(\tau_m/2 - \tau)$ vs. the optical depth $\tau(\Delta\lambda)$ for a contracting UFS. Ordinates are not to scale. (*b*) A plot of the line absorption coefficient φ_a vs. the abscissa x at a given $\Delta\lambda > 0$ for a contracting UFS (see eq. [14]). The optical depth at an abscissa $-x_0 < x < x_0$ is given by the area below the curve of φ_a between x and x_0 (see eq. [16]). The maximum of φ_a is at a positive abscissa x_m for all $\Delta\lambda > 0$, because $v_{ls} > 0$ for $x > 0$ and $v_{ls} < 0$ for $x < 0$. Therefore, the area between $x = 0$ and x_0, i.e., the optical depth τ_c of the center of the sphere, is greater than $\tau_m/2$, where τ_m is the total optical depth given by the area between $-x_0$ and x_0.

depth of order unity. For the pressures assumed in our model, this column depth implies a geometrical thickness of the absorption medium at least 1 order of magnitude larger than the characteristic dimension of the sphere. We conclude that unless the UFS pressures are significantly higher than those in our model, the hypothesis of continuum absorption must be abandoned.

The authors wish to thank the referee for his helpful comments and suggestions. This work was supported in part by the Italian Ministero dell'Università e della Ricerca Scientifica e Tecnologica, through the Astrophysical Observatory of Catania, and the Agenzia Spaziale Italiana (contract ASI-92-RS-53), and in part by NASA and ONR.

APPENDIX

To derive equation (18), we start from the symmetry property of the absorption profile function:

$$\varphi_a(\Delta\lambda, x) = \varphi_a(-\Delta\lambda, -x) . \tag{A1}$$

We note that equation (A1) holds not only for the assumed velocity field but also for any radial velocity field which is spherically symmetric around the center of the sphere. Using relation (A1) and equation (16), we have

$$\begin{aligned}\tau(-\Delta\lambda, x) &= \int_x^{x_0} \chi_0 \varphi_a(-\Delta\lambda, s)ds \\ &= -\int_x^{x_0} \chi_0 \varphi_a(\Delta\lambda, -s)d(-s) \\ &= \int_{-x_0}^{-x} \chi_0 \varphi_a[\Delta\lambda, (-s)]d(-s) \\ &= \tau_m(\Delta\lambda) - \tau(\Delta\lambda, -x) ,\end{aligned} \tag{A2}$$

where $\tau_m(\Delta\lambda) = \int_{-x_0}^{x_0} \chi_0 \varphi_a(\Delta\lambda, s)ds$. From equation (11) we have for a given line of sight

$$I(-\Delta\lambda) = \int_{-x_0}^{x_0} F_0(x)\varphi_a(-\Delta\lambda, x) \exp [-\tau(-\Delta\lambda, x)]dx .$$

Changing the integration variable to $w = -x$ and making use of relations (A1) and (A2) and the symmetry of the line contribution function $F_0(x)$ around the center of the sphere, yields

$$\begin{aligned}I(-\Delta\lambda) &= \int_{-x_0}^{x_0} F_0(w)\varphi_a(\Delta\lambda, w) \exp \{-[\tau_m(\Delta\lambda) - \tau(\Delta\lambda, w)]\}dw \\ &= \exp [-\tau_m(\Delta\lambda)] \int_{-x_0}^{x_0} F_0(w)\varphi_a(\Delta\lambda, w) \exp [\tau(\Delta\lambda, w)]dw .\end{aligned} \tag{A3}$$

Expressing the integrands in equations (11) and (A3) as functions of the optical depth τ along the given line of sight and noting that $d\tau = \chi_0 \varphi_a(\Delta\lambda, w)dw$ (see eq. [16]), we have, respectively,

$$I(\Delta\lambda) = \frac{1}{\chi_0} \int_0^{\tau_m} F_0(\tau) \exp (-\tau)d\tau , \tag{A4}$$

$$I(-\Delta\lambda) = \frac{\exp (-\tau_m)}{\chi_0} \int_0^{\tau_m} F_0(\tau) \exp (\tau)d\tau , \tag{A5}$$

where, for simplicity, the dependence on $\Delta\lambda$ has been dropped on the right-hand side, as will be done in the subsequent expressions. From equations (A4) and (A5) we have

$$\begin{aligned}\Delta I(\Delta\lambda) &= I(\Delta\lambda) - I(-\Delta\lambda) \\ &= \frac{1}{\chi_0} \int_0^{\tau_m} F_0(\tau)[\exp (-\tau) - \exp (-\tau_m) \exp (\tau)]d\tau \\ &= \frac{\exp (-\tau_m/2)}{\chi_0} \int_0^{\tau_m} F_0(\tau)[\exp (\tau_m/2 - \tau) - \exp (\tau - \tau_m/2)]d\tau \\ &= 2 \frac{\exp (-\tau_m/2)}{\chi_0} \int_0^{\tau_m} F_0(\tau) \sinh (\tau_m/2 - \tau)d\tau ,\end{aligned} \tag{A6}$$

which proves equation (18).

REFERENCES

Antiochos, S. K. 1984, ApJ, 280, 416
———. 1990, Mem. Soc. Astron. Italiana, 61(2), 369
Arnaud, M., & Rothenflug, R. 1985, A&AS, 82, 229
Athay, R. G. 1984, ApJ, 287, 412
Athay, R. G., & Dere, K. P. 1989, ApJ, 346, 514
Athay, R. G., & Holzer, T. E. 1982, ApJ, 255, 743
Ayres, T. R., et al. 1983, ApJ, 274, 801
Ayres, T. R., Jensen, E., & Engvold, O. 1988, ApJS, 66, 51
Blake, M. L., & Sturrock, P. A. 1985, ApJ, 290, 359
Boland, B. C., et al. 1975, MNRAS, 171, 697
Brueckner, G. E., Bartoe, J. D. F., Cook, J. W., Dere, K. P., & Socker, D. G. 1986, Adv. Space Res., 6(8), 263

Brueckner, G. E., & Moe, O. K. 1972, Space Res., 12, 1595
Cheng, C.-C., Doschek, G. A., & Feldman, U. 1979, ApJ, 227, 1037
Cheng, Q. Q. 1992a, A&A, 262, 581
———. 1992b, A&A, 266, 537
———. 1992c, A&A, 266, 549
Dere, K. P. 1982, Sol. Phys., 77, 77
———. 1989, ApJ, 340, 599
Dere, K. P., Bartoe, J.-D. F., & Brueckner, G. E. 1984, ApJ, 281, 870
Dere, K. P., Bartoe, J.-D. F., Brueckner, G. E., Cook, J. W., & Socker, D. G. 1987, Sol. Phys., 114, 223
Doschek, G. A., Feldman, U., & Bohlin, J. D. 1976, ApJ, 205, L177
Doschek, G. A., Feldman, U., van Hoosier, M. E., & Bartoe, J.-D. F. 1976, ApJS, 31, 417
Doschek, G. A., Strong, K. T., & Tsuneta, S. 1995, ApJ, 440, 370
Doyle, J. G., Raymond, J. C., Noyes, R. W., & Kingston, A. E. 1985, ApJ, 297, 816
Dragon, J. N., & Mutschlecner, J. P. 1980, ApJ, 239, 1045
Feldman, U. 1983, ApJ, 275, 367
———. 1987, ApJ, 320, 426
Feldman, U., Cohen, L., & Doschek, G. A. 1982, ApJ, 255, 325
Feldman, U., Doschek, G. A., & Patterson, N. P. 1976, ApJ, 209, 270
Fukao, S., Masayuki, U., & Takao, T. 1975, Rep. Ionos. Res. Japan, 29, 133
Gaetz, T. J., & Salpeter, E. E. 1983, ApJS, 52, 155
Gebbie, K. B., et al. 1981, ApJ, 251, L115
Gray, D. F. 1992, The Observation and Analysis of Stellar Photospheres (Cambridge Astrophys. Ser. 20; Cambridge: Cambridge Univ. Press)
Habbal, S. R., & Withbroe, G. L. 1981, Sol. Phys., 69, 77
Hassler, D. M., Rottman, G. J., Shoub, E. C., & Holzer, T. E. 1990, ApJ, 348, L77
Henze, W., & Engvold, O. 1992, Sol. Phys., 141, 51
Hummer, D. G., & Rybicki, G. B. 1982, ApJ, 254, 767
Klimchuk, J. A. 1987, ApJ, 323, 368
Landini, M., & Monsignori-Fossi, B. C. 1990, A&AS, 82, 229
Lites, B. W., Bruner, E. C., Chipman, E. G., Shine, R. A., Rottman, G. J., White, O. R., & Athay, R. G. 1976, ApJ, 210, L111
Mariska, J. T. 1988, ApJ, 334, 489
———. 1992, The Solar Transition Region (Cambridge Astrophys. Ser. 23; Cambridge: Cambridge Univ. Press)
McClymont, A. N. 1989, ApJ, 347, L47
McClymont, A. N., & Craig, I. J. D. 1987, ApJ, 321, 402
Meier, R. R. 1991, Space Sci. Rev., 58, 1
Parker, E. N. 1988, ApJ, 330, 474
———. 1989, Sol. Phys., 121, 271
Porter, J. G., Toomre, J., & Gebbie, K. B. 1984, ApJ, 238, 879
Priest, E. R. 1986, Sol. Phys., 104, 1
Raymond, J. C. 1979, ApJS, 39, 1
———. 1990, ApJ, 365, 387
Rybicki, G. B. 1984, in Methods in Radiative Transfer, ed. W. Kalkofen (Cambridge: Cambridge Univ. Press), 21
Spadaro, D., Noci, G., Zappalà, R. A., & Antiochos, S. K. 1990, ApJ, 355, 342
Sturrock, P. A. 1966, Nature, 211, 695
Sturrock, P. A., Dixon, W. W., Klimchuk, J. A., & Antiochos, S. K. 1990, ApJ, 356, L31
Vernazza, J. E., Avrett, E. H., & Loeser, R. 1976, ApJS, 30, 1